

Hydrogen Migration in the Phenylethen-2-yl Radical

Nigel W. Moriarty,[†] Nancy J. Brown,[‡] and Michael Frenklach^{*,†,‡}

Department of Mechanical Engineering, University of California at Berkeley, Berkeley, California 94720, and Energy and Environmental Technologies Division, Lawrence Berkeley Laboratory, Berkeley, California 94720

Received: May 5, 1999; In Final Form: July 2, 1999

The migration of hydrogen in the phenylethen-2-yl radical is investigated by determining optimal geometries and barrier and reaction energies using several quantum mechanical methods. Rate coefficients and equilibrium constants are obtained using the calculated data and RRKM theory. Theoretical methods compared include PM3, MP2, B3-LYP, CASPT2, and G2MP2. The applicability of these methods and comparisons with two others, G2M and CBS-RAD proposed to improve treatment of radicals, are discussed. The results obtained at the most reliable level of theory produce reaction rates sufficiently fast for these reactions to play a role in high-temperature aromatic chemistry.

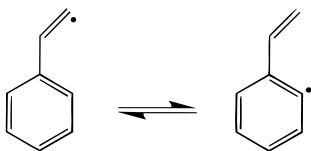
1. Introduction

The formation of soot in hydrocarbon combustion has important environmental consequences that recently are the subject of much scientific inquiry. Soot particles are nucleated from polycyclic aromatic hydrocarbon (PAH) precursors and accumulate most of their mass through surface reactions.^{1,2} Several reaction mechanisms have been suggested for the growth of PAHs and aromatic edges of soot particle surfaces.^{3–10}

Our recent computational study¹¹ identified a new class of reaction pathways for aromatic ring growth in combustion environments. The distinctive feature of the reaction pathways is the transfer of hydrogen atom between carbon atoms of the aromatic ring and those of the side chains. The calculations performed using the semiempirical quantum chemical PM3 method^{12,13} showed that hydrogen migration is sufficiently rapid to provide a more competitive alternative in many situations.

In the previous study,¹¹ a semiempirical level of quantum theory was chosen to screen a large number of mechanistic possibilities and to accommodate the large molecular size that is required for realistic modeling of PAH precursors and soot surfaces. Here, we turn to ab initio quantum mechanical theory to assess more accurately the feasibility of the hydrogen migration and to evaluate the earlier calculation.

The reaction chosen for this purpose is the one shown below:



The present choice was motivated by two considerations. First, H migration may play a direct role, since both the reactant and the product are known intermediates of aromatic growth in hydrocarbon flames. In the forward direction, the hydrogen in ring position 2 is transferred to the radical site on the side chain, thereby moving the radical vacancy from the side chain to the

ring. The addition of acetylene to the radical site of the product may form another aromatic ring. Second, reaction 1 is the smallest analogue of hydrogen transfer on large PAH molecules and soot particle surfaces, allowing one to study this class of reactions while remaining within the constraints of available computational power. In the case of a larger aromatic structure, when such a migration occurs at a bay site, the radical product may cyclize directly. We note that the hydrogen travels a relatively longer distance in the migration in reaction 1 compared to the migration in sterically crowded two- and three-ring compounds. Therefore, the reaction rate coefficients determined from this one-ring model should be a lower bound on the rate coefficients expected for the larger molecules.

At the present state of the art of computational quantum mechanics, the one-ring system is amenable to employing a spectrum of quantum chemical techniques, from the most simple to the complex. Evaluation of different methods is critical because, ultimately, we are interested in exploring the importance of new reaction paths in more complex, multi-ring systems. We want to investigate whether the application of lower levels of theory (i.e., PM3 and UHF) is useful. Furthermore, perturbation theories such as MP2 and MP4 have been employed in combustion modeling, and their performance is of interest as well. Density functional theory (DFT) has the attractive attribute of including correlation and scales favorably in comparison to other electron correlation methods. Moreover, DFT continues to improve and the approach referred to as Becke3 and Lee–Yang–Parr (B3-LYP) is considered most reliable. Multireference methods, which have been found to be particularly useful for treating radical reactions, were also considered. The G2MP2 method, although computationally intensive, provides chemical accuracy and is used to evaluate the other methods.

2. Quantum Mechanical Methods

Geometry optimization calculations on each of the minima associated with the two radicals and on the transition state were performed at several levels of theory. Unrestricted Hartree–Fock (UHF),¹⁴ second-order Møller–Plesset (MP2),¹⁵ and density functional theory (DFT), choosing the Becke3¹⁶ and Lee–Yang–Parr¹⁷ (B3-LYP) functionals, were used with two

* To whom correspondence should be addressed. Telephone: +1-510-643-1676. Fax: +1-510-642-6163. E-mail: myf@me.berkeley.edu.

[†] University of California at Berkeley.

[‡] Lawrence Berkeley Laboratory.

TABLE 1: Geometry Computed for the Reactant Molecule at Various Levels of Theory and Using Various Basis Sets^a

| method | geometry parameters | | | | | | | | | | | |
|----------------------|---------------------|-------|-------|-------|-------|-------|-------|-------|-------|-------|-------|------|
| | r1 | r2 | r3 | r4 | r5 | r6 | r7 | a1 | a2 | a3 | a4 | d1 |
| AM1 | 1.399 | 1.445 | 1.315 | 1.099 | 1.110 | 1.060 | 2.926 | 121.3 | 124.6 | 161.5 | 115.9 | 0.0 |
| PM3 | 1.395 | 1.449 | 1.321 | 1.095 | 1.101 | 1.065 | 2.898 | 121.3 | 122.9 | 157.3 | 117.4 | 0.0 |
| HF/3-21G | 1.398 | 1.449 | 1.353 | 1.072 | 1.080 | 1.068 | 2.986 | 122.1 | 125.5 | 133.8 | 116.1 | 0.0 |
| HF/6-31G(d) | 1.400 | 1.450 | 1.354 | 1.075 | 1.082 | 1.071 | 3.004 | 122.2 | 126.1 | 133.2 | 117.7 | 0.0 |
| HF/6-31G(d,p) | 1.401 | 1.450 | 1.353 | 1.075 | 1.082 | 1.071 | 3.004 | 122.2 | 126.1 | 133.4 | 116.3 | 0.0 |
| B3-LYP/3-21G | 1.396 | 1.479 | 1.318 | 1.084 | 1.097 | 1.080 | 3.004 | 121.7 | 126.5 | 137.1 | 118.9 | 0.0 |
| B3-LYP/6-31G(d) | 1.395 | 1.474 | 1.312 | 1.087 | 1.099 | 1.082 | 3.018 | 121.8 | 127.2 | 136.7 | 117.9 | 0.0 |
| B3-LYP/6-31G(d,p) | 1.395 | 1.474 | 1.319 | 1.086 | 1.098 | 1.081 | 3.018 | 121.9 | 127.3 | 137.0 | 115.0 | 0.0 |
| B3-LYP/6-311G(d,p) | 1.392 | 1.474 | 1.314 | 1.084 | 1.097 | 1.079 | 3.019 | 121.9 | 127.5 | 137.8 | 117.6 | 0.0 |
| MP2/3-21G | 1.410 | 1.505 | 1.295 | 1.087 | 1.094 | 1.081 | 3.133 | 120.8 | 124.1 | 135.7 | 115.8 | 54.0 |
| MP2/6-31G(d) | 1.403 | 1.489 | 1.284 | 1.087 | 1.096 | 1.081 | 3.050 | 121.0 | 125.1 | 136.8 | 116.2 | 39.2 |
| MP2(Full)/6-31G(d) | 1.402 | 1.488 | 1.282 | 1.087 | 1.096 | 1.080 | 3.044 | 119.7 | 125.1 | 136.8 | 116.2 | 38.3 |
| MP2/6-31G(d,p) | 1.402 | 1.491 | 1.283 | 1.083 | 1.092 | 1.077 | 3.054 | 121.2 | 125.4 | 136.4 | 116.2 | 38.1 |
| CASSCF(7,7)/6-31G(d) | 1.390 | 1.480 | 1.308 | 1.075 | 1.082 | 1.071 | 3.004 | 121.9 | 126.6 | 134.1 | 117.8 | 0.0 |
| G2MP2 | 1.365 | 1.497 | 1.289 | 1.086 | 1.095 | 1.080 | 2.990 | 121.7 | 126.3 | 136.2 | 115.0 | 0.0 |

^a The bond lengths represented by r1–r7 are in angstroms and angles represented by a1–a4 and d1 are in degrees. The internal coordinate numbering system is defined in Figure 1.

standard basis sets. A small basis set, 3-21G, provided quick convergence to an optimized geometry, and the larger basis set, 6-31G(d,p), was used to determine the final geometries, frequencies, and energies. An additional calculation using the triple- ζ basis set, 6-311G(d,p), and the B3-LYP method was performed to compare with the geometry optimization step of the G2M method.¹⁸ Similarly, the 6-31G(d) basis set was included because of its use in the optimization step of the CBS-RAD^{19,20} and G2MP2 methods.²¹ Multireference methods were represented by the complete active space SCF, CASSCF,²² using seven orbitals as the active space and including seven electrons, with two single-point correlation methods using the CASSCF wave function: CASMP2,²³ an MP2 correlation inclusion method, and CASPT2(g2).²⁴ Two semiempirical quantum methods, AM1²⁵ and PM3,^{12,13} were used. The PM3 calculation was the subject of a previous study.¹¹ The stationary points were correctly characterized regarding the number of imaginary frequencies, one for the transition state and none for the local minima. A calculation following the reaction path using the intrinsic reaction coordinate (IRC) was performed using the PM3 method to confirm the reaction pathway.

Composite methods use several calculation steps combined, using formulas determined from comparison with experimental values to improve results. The first composite chemistry method used was the complete basis set method, CBS-4,²⁶ using an UHF/3-21G(d) optimization and frequency step and a series of three single-point calculations to improve the energies. These are MP4/6-31G, MP2/6-31+(d',p'), and HF/CBS-B1, which is the largest basis in the calculation. This is one of the simplest of the CBS group of methods. The second composite method, designed to give chemical accuracy, known as the G2 method,²⁷ has recently been modified into various incarnations for application to larger molecules. One of these, the G2MP2 method,²¹ was used as the highly accurate benchmark method in this study.

The G2MP2 method commences with a geometry and frequencies determination using the HF method and the standard 6-31G(d) basis set. By use of the final HF geometry, a further MP2 optimization including all the core electrons {MP2(Full)} is performed. A quadratic correlation interaction, singles, doubles, and approximate triples (QCISD[T])²⁸ and the 6-311G-(d,p) basis set calculation at the final optimized geometry determine the base energy for the G2MP2 energy. Several corrections for basis set superposition error (BSSE), unpaired electrons, and frequency errors are included. First, the difference

in MP2 energies using the 6-311+G(3df,2d) and 6-311G(d,p) as a measure of the BSSE error is included. Second, a zero-point energy (ZPE) correction is determined using the HF/6-31G(d) frequencies scaled by 0.893.²¹ Last, a further empirical adjustment is made for unpaired electrons using the formula²¹ $-4.81n_{\beta} - 0.19n_{\alpha}$ where $n_{\alpha} \geq n_{\beta}$, n_{α} and n_{β} are the number of α and β spin electrons, respectively, and the units are millihartree. The method is reported to be accurate to 3 kcal/mol.²¹

The quantum chemical calculations were performed using the GAUSSIAN94,²⁹ MOLCAS 4,³⁰ and MOPAC 93³¹ suites of codes on PowerMac, AIX RS/6000, Pentium II (Linux), and CRAY J90 computers.

3. Quantum Mechanical Results

3.1. Geometry. It is conceivable that the acetylene adducts in both the reactant and the product will rotate out of the plane of the six-member carbon ring to reduce repulsion. Therefore, the initial geometry for all optimization calculations had a value for the dihedral angle of the carbon in the side chain to the plane of the carbon ring (denoted d1 in Tables 1–3) set to 45°. In this fashion, a higher symmetry was not imposed on the molecules. The nonzero dihedral angle was also used in the transition-state calculations, but in all cases the optimized molecule was planar.

Key internal coordinate results for each of the optimized reactant stationary points are given in Table 1. A diagram of the transition state including internal coordinate nomenclature given in Figure 1 also defines the geometry nomenclature for the reactant. As indicated, the most striking feature is the predicted planarity of the reactant. Only the MP2 geometry optimizations retained a nonzero dihedral angle, denoted d1 in Table 1 for the acetylene adduct. To investigate whether this is at all reasonable, we examine the geometry of styrene, the nonradical counterpart obtained from the addition of a hydrogen to the radical site. Hartree–Fock calculations^{32–35} give a very low torsional barrier, 0.21 kcal/mol, and a nonplanar optimized geometry with a 15–20° torsion angle. An MP2/6-31G(d) optimization of the styrene molecule produced a dihedral angle of 27.6°, indicating that the MP2 procedure predicts larger dihedral angles than the Hartree–Fock calculations.

The values for the dihedral angle in the reactant radical, d1, using the MP2 method range between 38° and 54°, somewhat larger than the styrene case. Furthermore, single-point calculations on the planar and nonplanar geometries using the QCISD-

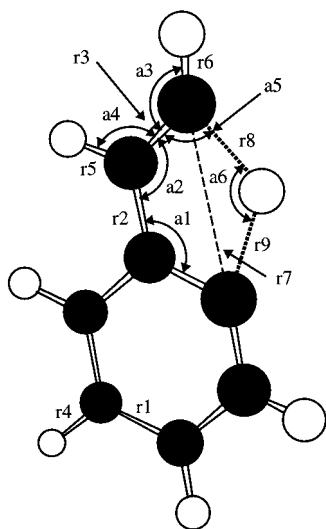


Figure 1. Molecular geometry diagram displaying the internal coordinate numbering system used in Tables 1–3.

[T] method show that all post-HF methods favor the nonplanar geometry by 3.6 (PMP3) to 6.5 kcal/mol (QCISD[T]).

The G2MP2 method gives an in-plane result regardless of the MP2(Full) optimization calculation performed as part of this procedure. This outcome can be traced to the MP2(Full) calculation step using the Hartree–Fock optimized geometry as its initial geometry. There is a small barrier to rotation of the acetylene adduct, even though the symmetry is C_1 , which hinders the G2MP2 method's MP2 optimization from obtaining the out-of-plane result. Torsional barriers for styrene³³ were calculated as 0.21 kcal/mol with the MP2/6-311G(d,p)//HF/6-31G(d) potential energy surface (PES). The optimized angle has a large effect on the MP2(Full) energy component, 20.96 kcal/mol but only 2.30 kcal/mol for the spin-corrected PMP2-(Full) energies. The zero-point energy correction does not change this result substantially. Because the transition state is not affected by differing optimized geometries dependent on the initial geometry, the reaction barrier is reduced in the MP2 correction term of the G2MP2 computation when the planar reactant geometry is used.

The bond length, r_7 , in Table 1 gives the distance between the two carbon–hydrogen bond sites for the migrating hydrogen. These lengths are obviously larger in the MP2 results because of the out-of-plane geometry, but the increase is not simply proportional to the angular increase. The MP2/6-31G(d,p) case gives an in-plane distance of 2.4 Å compared to the UHF/6-31G(d,p) result of 3.0 Å. The UHF geometry has strained bond angles as indicated by the larger results for angles a_1 and a_2 .

The predicted geometries for the product radical are summarized in Table 2; the corresponding internal coordinate nomenclature can be determined from Figure 1. The out-of-plane dihedral angle is calculated to be much smaller than the reactant, but once again, only the MP2 methods predict nonzero results. Perturbations on this are the G2MP2 and PM3 results. For the G2MP2 calculation, the MP2(Full)/6-31G(d) optimization starting from the in-plane UHF/6-31G(d) configuration predicted an out-of-plane angle of 2.93°. Apparently, there is a much lower barrier to rotation, if at all, or a very broad valley on the PES. For the PM3 computation, the out-of-plane angle was 0.05°, hardly a significant amount. The C–C and C–H bonds exhibit similar changes when a larger basis set or a correlation method is used when compared to the reactant geometry results.

One overall difference between the reactant and the product radical is the angle, a_3 , that the hydrogen on the end of the chain makes with the last C–C bond. The reactant value is between 15° and 40° larger than the value for a_3 in the product. In the product, the endmost hydrogen is repelled more strongly by the other hydrogen, as indicated by the slightly smaller angle a_3 .

Another small difference between the reactant and the product radicals is the angle, a_1 , that the adduct makes with the ring. In all cases, the calculations predict a larger angle for the product by about 3°. The radical site is on the ring in the product, and analysis of other geometry values including the lengthening of the C–C bond in the ring, r_1 , shows that the radical carbon has collapsed inward because of loss of benzene ring conjugation.

The transition-state diagram and geometric results are given in Figure 1 and Table 3, respectively. All of the methods predict a planar structure except for a very small angle for the MP2-(Full) method. Several of the methods predict the position of the migrating hydrogen to be out of the plane of the molecule, but the angle subtended at the transition ring carbons is less than 1°. The semiempirical methods have the greatest change in the geometry of the ring associated with the transition state, namely, the angle that the migrating hydrogen subtends with respect to the donor and acceptor carbons. The angle subtended with the acceptor carbon, a_5 , is greater by more than 5°, possibly a significant variation.

3.2. Energetics. Calculated reaction energetics are given in Table 4. Results from the G2MP2 sequence of calculations are included at the bottom of the table. For example, the method designated MP2(Full)planar/6-31G(d) is a constrained optimized energy starting from the UHF/6-31G(d) geometry, the superscript “planar” referring to the planar geometry of the reactant obtained from a C_s symmetry constrained optimization. Frequencies taken from the UHF/6-31G(d) calculation are used to determine the reaction rate coefficients for these energies.

The Hartree–Fock method uniformly produces barrier energies over 50 kcal/mol but gives a wide range of reaction energies. The lowest barrier is predicted by the MP2(Full)planar/6-31G(d) method. This is not unexpected, since the geometry of the reactant has not been fully optimized, thus yielding a somewhat higher energy.

The CASSCF(7,7)/6-31G(d) barrier energy is slightly less than the HF results at 43.99 kcal/mol, consistent with the wave function being almost single reference. The largest weight attributed to a reference electron configuration other than the ground state is less than 0.1, implying the wave function is dominated by the ground-state configuration. This is also the case for the CASPT2 wave function that predicts a much lower value, 28.52 kcal/mol, for the barrier height, very similar to the G2MP2 barrier energy. The CASMP2 barrier energy is similar to the CASPT2 result, but the reaction energy is nearly 20 kcal/mol lower. This may be due to the valence bond expansion of the MP2 procedure in the CASSCF active space altering the effective active space on the product radical. The CBS-4 barrier energy is 6 kcal/mol lower than the G2MP2 values and results in good agreement with the G2(P)MP2planar. This similarity may be traced to the planar configuration of the molecule predicted by the CBS-4 method; however, there is far less electron correlation included in the post-HF treatment of this method compared to the G2MP2 formalism. The planar geometry of the reactant is due to the initial HF optimization step that is common to all the CBS methods. Subsequent optimization in the other CBS methods would likely remain in

TABLE 2: Geometric Results for the Product Molecule at Various Levels of Theory and Using Various Basis Sets^a

| method | geometry results | | | | | | | | | | | | | |
|----------------------|------------------|-------|-------|-------|-------|-------|-------|-------|-------|-------|-------|-------|-------|-----|
| | r1 | r2 | r3 | r4 | r5 | r6 | r7 | r8 | a1 | a2 | a3 | a4 | a5 | d1 |
| AM1 | 1.409 | 1.438 | 1.347 | 1.098 | 1.104 | 1.097 | 2.970 | 1.098 | 124.4 | 123.9 | 121.8 | 115.6 | 122.3 | 0.0 |
| PM3 | 1.403 | 1.444 | 1.342 | 1.094 | 1.097 | 1.085 | 2.945 | 1.081 | 123.9 | 123.0 | 122.4 | 116.2 | 122.8 | 0.1 |
| HF/3-21G | 1.406 | 1.447 | 1.355 | 1.072 | 1.075 | 1.072 | 3.006 | 1.073 | 123.6 | 125.3 | 121.1 | 115.9 | 121.9 | 0.0 |
| HF/6-31G(d) | 1.404 | 1.450 | 1.356 | 1.075 | 1.078 | 1.074 | 3.022 | 1.075 | 123.8 | 125.7 | 120.9 | 118.5 | 122.0 | 0.0 |
| HF/6-31G(d,p) | 1.406 | 1.459 | 1.347 | 1.076 | 1.078 | 1.075 | 3.020 | 1.076 | 123.9 | 125.6 | 120.9 | 115.7 | 121.9 | 0.0 |
| B3-LYP/3-21G | 1.397 | 1.472 | 1.337 | 1.084 | 1.088 | 1.084 | 3.023 | 1.086 | 124.1 | 125.2 | 121.6 | 119.7 | 121.5 | 0.0 |
| B3-LYP/6-31G(d) | 1.396 | 1.469 | 1.339 | 1.087 | 1.090 | 1.086 | 3.034 | 1.087 | 124.4 | 125.7 | 121.3 | 119.2 | 121.7 | 0.0 |
| B3-LYP/6-31G(d,p) | 1.407 | 1.469 | 1.338 | 1.087 | 1.089 | 1.085 | 3.033 | 1.086 | 124.4 | 125.6 | 121.3 | 115.2 | 121.6 | 0.3 |
| B3-LYP/6-311G(d,p) | 1.393 | 1.468 | 1.335 | 1.084 | 1.087 | 1.083 | 3.034 | 1.085 | 124.5 | 125.8 | 121.2 | 119.1 | 121.6 | 0.0 |
| MP2/3-21G | 1.434 | 1.464 | 1.333 | 1.087 | 1.091 | 1.085 | 3.032 | 1.087 | 124.2 | 125.4 | 121.7 | 115.5 | 121.7 | 9.5 |
| MP2/6-31G(d,p) | 1.419 | 1.450 | 1.328 | 1.083 | 1.086 | 1.080 | 3.008 | 1.081 | 124.5 | 125.2 | 121.2 | 115.7 | 121.3 | 5.8 |
| CASSCF(7,7)/6-31G(d) | 1.395 | 1.478 | 1.321 | 1.075 | 1.078 | 1.075 | 3.022 | 1.076 | 123.4 | 125.9 | 121.1 | 119.0 | 122.2 | 0.0 |
| G2MP2 | 1.379 | 1.496 | 1.295 | 1.087 | 1.089 | 1.084 | 3.005 | 1.086 | 123.9 | 125.3 | 121.5 | 114.5 | 122.0 | 2.9 |

^a The bond lengths represented by r1–r8 are in angstrom and angles represented by a1–a5 and d1 are in degrees. The internal coordinate numbering system is defined in Figure 1.

TABLE 3: Geometric Results for the Transition State at Various Levels of Theory and Using Various Basis Sets^a

| method | geometry results | | | | | | | | | | | | | | | |
|----------------------|------------------|-------|-------|-------|-------|-------|-------|-------|-------|-------|-------|-------|-------|-------|-------|-----|
| | r1 | r2 | r3 | r4 | r5 | r6 | r7 | r8 | r9 | a1 | a2 | a3 | a4 | a5 | a6 | d1 |
| AM1 | 1.411 | 1.470 | 1.337 | 1.099 | 1.093 | 1.076 | 2.366 | 1.369 | 1.392 | 108.4 | 109.6 | 138.2 | 122.2 | 103.7 | 118.0 | 0.0 |
| PM3 | 1.405 | 1.470 | 1.337 | 1.095 | 1.090 | 1.078 | 2.362 | 1.379 | 1.418 | 108.8 | 109.1 | 135.9 | 122.8 | 105.4 | 115.3 | 0.0 |
| HF/3-21G | 1.410 | 1.471 | 1.329 | 1.072 | 1.072 | 1.067 | 2.459 | 1.438 | 1.378 | 110.0 | 112.3 | 134.8 | 122.8 | 98.4 | 121.6 | 0.0 |
| HF/6-31G(d) | 1.379 | 1.483 | 1.339 | 1.076 | 1.076 | 1.071 | 2.442 | 1.382 | 1.404 | 110.0 | 111.1 | 133.1 | 125.6 | 99.3 | 122.5 | 0.0 |
| HF/6-31G(d,p) | 1.403 | 1.484 | 1.338 | 1.076 | 1.076 | 1.072 | 2.437 | 1.378 | 1.400 | 109.9 | 111.0 | 132.9 | 123.4 | 99.4 | 122.6 | 0.0 |
| B3-LYP/3-21G | 1.394 | 1.488 | 1.333 | 1.084 | 1.085 | 1.080 | 2.467 | 1.401 | 1.402 | 110.6 | 111.8 | 134.6 | 125.7 | 98.4 | 123.9 | 0.0 |
| B3-LYP/6-31G(d) | 1.393 | 1.480 | 1.333 | 1.087 | 1.089 | 1.083 | 2.451 | 1.391 | 1.385 | 109.9 | 111.8 | 134.0 | 125.4 | 98.1 | 124.0 | 0.0 |
| B3-LYP/6-31G(d,p) | 1.413 | 1.480 | 1.332 | 1.087 | 1.088 | 1.083 | 2.449 | 1.387 | 1.383 | 109.8 | 111.7 | 133.9 | 122.9 | 98.0 | 125.3 | 0.0 |
| B3-LYP/6-311G(d,p) | 1.390 | 1.483 | 1.327 | 1.084 | 1.086 | 1.081 | 2.449 | 1.390 | 1.384 | 109.7 | 111.8 | 134.8 | 125.6 | 98.1 | 124.0 | 0.0 |
| MP2/3-21G | 1.423 | 1.500 | 1.307 | 1.087 | 1.087 | 1.081 | 2.468 | 1.402 | 1.404 | 109.5 | 112.2 | 134.6 | 122.4 | 99.1 | 123.3 | 0.0 |
| MP2/6-31G(d) | 1.399 | 1.479 | 1.298 | 1.087 | 1.089 | 1.083 | 2.426 | 1.378 | 1.368 | 109.2 | 111.9 | 134.9 | 125.7 | 98.7 | 124.1 | 0.0 |
| MP2/6-31G(d,p) | 1.397 | 1.479 | 1.297 | 1.083 | 1.084 | 1.079 | 2.415 | 1.370 | 1.354 | 108.9 | 111.7 | 134.4 | 125.4 | 98.5 | 124.9 | 0.0 |
| CASSCF(7,7)/6-31G(d) | 1.385 | 1.484 | 1.339 | 1.075 | 1.075 | 1.072 | 2.406 | 1.363 | 1.367 | 108.8 | 110.5 | 133.0 | 125.9 | 99.6 | 123.6 | 0.0 |
| G2MP2 | 1.407 | 1.480 | 1.295 | 1.088 | 1.089 | 1.082 | 2.427 | 1.385 | 1.366 | 109.2 | 112.0 | 134.5 | 122.7 | 98.7 | 123.9 | 0.1 |

^a The bond lengths represented by r1–r9 are in angstroms and angles represented by a1–a6 and d1 are in degrees. The internal coordinate numbering system is defined in Figure 1.

the planar configuration similar to the G2MP2 procedure unless there was intervention.

The barrier energies for the remainder of the methods are in the 20–35 kcal/mol range except for the AM1 method and the methods designated UMP2(Full)/6-31G(d) and PMP2(Full)/6-31G(d). The first is a parametrized semiempirical method that is postdated by the PM3 method.

The reaction energies have a smaller range, although the UHF/6-31G(d,p) is remarkably large at 13.35 kcal/mol. Both semiempirical methods determine reaction energies in this region with the PM3 result of 5.56 kcal/mol being remarkably similar to the G2MP2 values. This is most likely fortuitous given the predicted planar geometry of the PM3 method.

3.3. Spin Contamination. The expectation values of the spin-squared operator, $\langle S^2 \rangle$, for each method are given in Table 5. The values should be 0.75 for the doublet state. The density functional methods perform very well in this regard, and the CAS calculations also have good spin results especially for the reactant and product radicals. The largest deviation, except for HF methods, is for the MP2(Full) calculations. Spin contamination may be the reason for high values of energy barriers and reaction energies. By even the most lenient standards, the spin contamination for the MP2(Full) is too large. Also, the results for the CBS-4 method are not good.

3.4. Compound Methods. The incomplete geometry optimization of the reactant species in the G2MP2 leads to errors in the energetics. The difference in barrier energies between

TABLE 4: Barrier and Reaction Energies in kcal/mol for Various Levels of Theory and Basis Sets^a

| method | barrier energy | reaction energy |
|--|----------------|-----------------|
| AM1 | 38.23 | 6.01 |
| PM3 | 29.36 | 5.56 |
| HF/3-21G | 50.65 | 1.50 |
| HF/6-31G(d,p) | 52.93 | 13.27 |
| B3-LYP/3-21G | 28.01 | 0.99 |
| B3-LYP/6-31G(d,p) | 26.93 | 0.72 |
| B3-LYP/6-311G(d,p) | 27.50 | 1.09 |
| UMP2/3-21G | 34.24 | 0.46 |
| PMP2/3-21G | 30.84 | 4.18 |
| UMP2/6-31G(d,p) | 30.00 | -1.27 |
| PMP2/6-31G(d,p) | 27.33 | 1.84 |
| CBS-4 | 22.84 | 3.76 |
| CASSCF(7,7)/6-31G(d) | 43.99 | -1.09 |
| CASPT2(7,7)/6-31G(d) | 28.52 | -0.36 |
| CASMP2(7,7)/6-31G(d) | 29.90 | -20.14 |
| G2MP2 Components | | |
| HF ^{planar} /6-31G(d) | 53.91 | 1.00 |
| UMP2(Full) ^{planar} /6-31G(d) | 11.10 | 2.90 |
| PMP2(Full) ^{planar} /6-31G(d) | 26.70 | 1.88 |
| UMP2(Full)/6-31G(d) | 54.44 | 24.74 |
| PMP2(Full)/6-31G(d) | 41.98 | 9.56 |
| G2PMP2 ^{planar} | 24.76 | 1.83 |
| G2PMP2 | 28.93 | 6.00 |
| G2MP2 ^{planar} | 23.11 | 0.39 |
| G2MP2 | 28.35 | 5.63 |

^a Zero-point energy corrections are included in all results except for AM1 and PM3.

TABLE 5: Spin Eigenvalues for Several Methods and Basis Sets Used in the Work^a

| method | reactant | product | transition |
|--|----------|---------|------------|
| HF/3-21G | 1.83 | 1.86 | 1.63 |
| HF/6-31G(d,p) | 1.83 | 1.37 | 1.06 |
| B3-LYP/3-21G | 0.77 | 0.76 | 0.76 |
| B3-LYP/6-31G(d) | 0.77 | 0.76 | 0.76 |
| B3-LYP/6-31G(d,p) | 0.77 | 0.76 | 0.76 |
| B3-LYP/6-311G(d,p) | 0.76 | 0.76 | 0.76 |
| UMP2/3-21G | 0.98 | 0.89 | 1.02 |
| UMP2/6-31G(d,p) | 0.94 | 0.86 | 0.96 |
| CBS-4 | 1.76 | 1.78 | 1.03 |
| CASSCF(7,7)/6-31G(d) | 0.79 | 0.88 | 1.10 |
| G2MP2 Components | | | |
| HF/6-31G(d) | 1.83 | 1.84 | 1.07 |
| UMP2(Full) ^{planar} /6-31G(d) | 1.46 | 1.48 | 1.24 |
| UMP2(Full)/6-31G(d) | 0.94 | 1.48 | 1.24 |
| QCISD ^{planar} /6-311G(d,p) | 0.93 | 0.87 | 0.94 |
| QCISD/6-311G(d,p) | 0.89 | 0.87 | 0.94 |

^a The exact value is 0.75.

the planar reactant and the nonplanar reactant is significant with the restricted results differing by less (4 kcal/mol) than the unrestricted values (7 kcal/mol). A more recent compound method, CBS-RAD,^{19,20} has been proposed to give a more uniform and accurate treatment to radicals. The geometry optimization is performed at either the QCISD/6-31G(d) or the B3-LYP/6-31G(d) levels. However, computational resources are a consideration, so the CBS-RAD calculations were not pursued because of the computational demands of the first optimization approach and the planar geometry resulting from the second. A third approach using a QCISD/6-31G(d) optimization and the zero-point energy correction from the B3-LYP/6-31G(d) level is problematic because of the differing geometries (nonplanar and planar, respectively) obtained for each calculation. As is often the case with compound methods, the single-point calculations are the limiting factor in any CBS-RAD calculation. It is important to note that a recent revision²⁰ using various reductions in correlation and basis set sizes may be promising for large radicals.

Despite the geometry differences, the final G2(P)MP2^{planar} and G2(P)MP2 results are remarkably similar, especially when the restricted and unrestricted results are compared. The restricted G2MP2 method, designated G2PMP2, uses the restricted MP2 values to determine the BSSE correction. If the post-MP2/6-31G(d) corrections were constant, the energy barrier for the nonplanar reactant would be 44 kcal/mol. The QCISD-(T) calculation (and included MP2 computation) does not give uniform corrections to the final result for the planar and nonplanar reactants.

4. Methodological Choices

One objective of the present study is to assess the various quantum mechanical methods to determine viable choices for the kinetics of the type and molecular size of the reactions considered here. One criterion for selecting a method is its theoretical foundation. In situations such as reaction 1, when no experimental data are available for comparison, the rigorous theoretical underpinnings of methods with seemingly close results can serve as a basis for choosing a more reliable method. Another criterion is the performance of a method established by a large number of different experimental comparisons. An overriding concern is the demand on computational resources and expense that can limit the level of sophistication attainable.

The methods investigated can be divided into five groups: semiempirical, single-reference, multireference, DFT, and com-

pound methods. This division is somewhat arbitrary and nonexclusive but serves to discuss the choices available.

One of the semiempirical methods tested, PM3, showed seemingly close agreement with the higher level method. However, as pointed out earlier in the discussion, this result is most likely fortuitous. Nonetheless, this does not preclude using PM3 as a reconnaissance tool especially for molecules too large for other methods. The single-reference method, MP2, provided a better geometry optimization than all the methods explicitly tested in our calculations for stationary points. Perturbation techniques applied to a multireference wave function, in particular CASPT2, also produced barriers in good agreement with the G2MP2 and the MP2 methods. Similar agreement was obtained with the B3-LYP DFT method. All three required a large basis set to ensure accuracy.

By use of the criteria discussed, the method of choice is G2MP2. Taking into account the systematic approach of the G2MP2 method to reduce the errors associated with BSSE, unpaired electrons, and frequencies, we assume it to be the most reliable method with the added precaution of requiring the restarting of the MP2 optimization with a nonplanar geometry. In addition, the G2MP2 method has proven reliable for a large range of calculations including the G2 data set²⁷ and produces reasonable electronic spin results for all stationary points in this reaction. Other compound methods could also be used depending on the computer resources available.

5. Kinetics Results

Evaluation of the rate for the hydrogen transfer in the phenylethen-2-yl is important to the understanding of soot formation. Unfortunately, there is no experimental data available for this or similar reactions, and hence, we must rely solely on quantum mechanical predictions to provide the required information. In light of this, we calculate the rate coefficients and equilibrium constants using a sample of the quantum mechanical methods to assess further their performance and how the sensitivity of the evaluation of the rate coefficients and equilibrium constants differs in the quantum mechanical results. The reaction rate falloff calculations are performed with our top choice, the G2MP2 results.

5.1. Calculation Details. The reaction barriers and conventionally scaled frequencies³⁶ were used to determine the Rice–Ramsperger–Kassel–Marcus (RRKM)^{37,38} rate coefficients for both the forward and reverse directions of reaction 1. The moments of inertia were taken from the present calculations at the optimized geometries and the Lennard-Jones parameters from empirically determined formulas.³⁹ Following Gilbert and Smith,³⁸ the real frequencies below 150 cm⁻¹ were examined by graphically visualizing the associated normal mode vibrations to identify internal rotational modes that were subsequently treated as free rotors.

5.2. Rate Coefficients. The data (energies, geometries, and frequencies) obtained in the quantum mechanical calculations were used to compute the rate coefficients of reaction 1 using the RRKM treatment. The high-pressure limit rate coefficients of reaction 1 for the forward direction calculated using data from various theoretical methods are displayed in Figures 2–4. The corresponding Arrhenius fits are given in Table 6.

The effect of spin contamination on the calculated rate coefficients is shown in Figure 2. The spin-projected rate coefficients are larger than the corresponding unrestricted computations with the same basis set by almost an order of magnitude at 1000 K, reducing to less than half that amount at

TABLE 6: Rate Coefficients and Equilibrium Constants Obtained for Various Methods and Basis Sets

| method | $k_{\infty} = AT^n \exp(-\theta/T)$ | | | $K_{\text{eq}} = A \exp(-\theta/T)$ | |
|--|-------------------------------------|-------|--------------|-------------------------------------|--------------|
| | $A \times 10^{-9} (\text{s}^{-1})$ | n | θ (K) | A | θ (K) |
| AM1 | 3.66 | 0.618 | 19200 | 0.404 | 2650 |
| PM3 | 5.51 | 0.617 | 14800 | 0.455 | 2420 |
| HF/3-21G | 12.4 | 0.673 | 25900 | 1.004 | 668 |
| HF/6-31G(d,p) | 4.72 | 0.642 | 26500 | 0.591 | 6310 |
| B3-LYP/3-21G | 12.1 | 0.673 | 14600 | 0.833 | 316 |
| B3-LYP/6-31G(d) | 8.19 | 0.670 | 14400 | 0.848 | 85.3 |
| B3-LYP/6-31G(d,p) | 10.1 | 0.685 | 14000 | 0.845 | 186 |
| B3-LYP/6-311G(d,p) | 13.1 | 0.580 | 14300 | 0.835 | 367 |
| UMP2/3-21G | 8.40 | 0.652 | 17600 | 0.934 | 97.3 |
| PMP2/3-21G | 9.12 | 0.643 | 15800 | 0.921 | 1950 |
| UMP2/6-31G(d,p) | 9.23 | 0.639 | 15300 | 0.673 | -904 |
| PMP2/6-31G(d,p) | 8.18 | 0.652 | 14000 | 0.661 | 649 |
| CBS-4 | 5.28 | 0.636 | 11500 | 1.443 | 1800 |
| CASSCF(7,7)/6-31G(d) | 23.8 | 0.632 | 22800 | 1.015 | -708 |
| CASPT2/6-31G(d) | 17.1 | 0.669 | 15000 | 1.014 | -343 |
| G2MP2 Components | | | | | |
| HF/6-31G(d) | 7.93 | 0.581 | 27200 | 0.978 | 400 |
| UMP2(Full) ^{planar} /6-31G(d) | 5.77 | 0.627 | 5560 | 0.986 | 1360 |
| PMP2(Full) ^{planar} /6-31G(d) | 6.94 | 0.607 | 13500 | 0.987 | 844 |
| G2PMP2 ^{planar} | 5.49 | 0.632 | 12400 | 0.992 | 815 |
| G2PMP2 | 5.12 | 0.632 | 14500 | 0.926 | 2610 |
| G2MP2 ^{planar} | 5.47 | 0.632 | 11600 | 0.993 | 93.5 |
| G2MP2 | 5.23 | 0.629 | 14200 | 0.925 | 2720 |

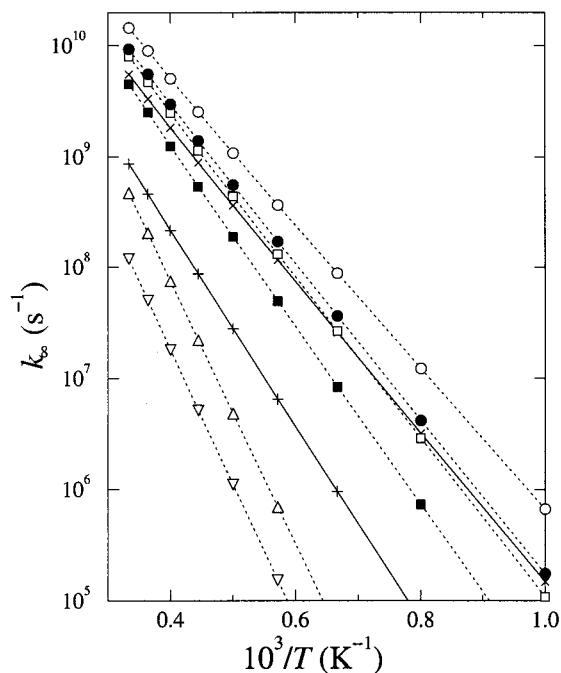


Figure 2. High-pressure-limit rate coefficients of the forward reaction 1, k_{∞} , comparing the UMP2/6-31G(d,p) {solid circle, dashed line}, PMP2/6-31G(d,p) {open circle, dashed line}, UMP2/3-21G {solid square, dashed line}, and PMP2/3-21G {open square, dashed line} results. Hartree–Fock results for the 3-21G {open up triangle, dashed line} and 6-31G(d,p) {open down triangle, dashed line} basis sets and semiempirical methods AM1 {plus, solid line} and PM3 {times, solid line} are included.

2500 K. This is a direct reflection of the lower predicted energy barrier using the PMP2 method.

Figure 2 also illustrates the semiempirical and Hartree–Fock reaction rate coefficients. The HF rate coefficients are less than the MP2 results. The AM1 rate coefficient is similar to the HF results, while the PM3 rate coefficient is more similar to the MP2 values. This agreement is, once again, most likely a cancellation of errors, especially considering the differences in computed geometries.

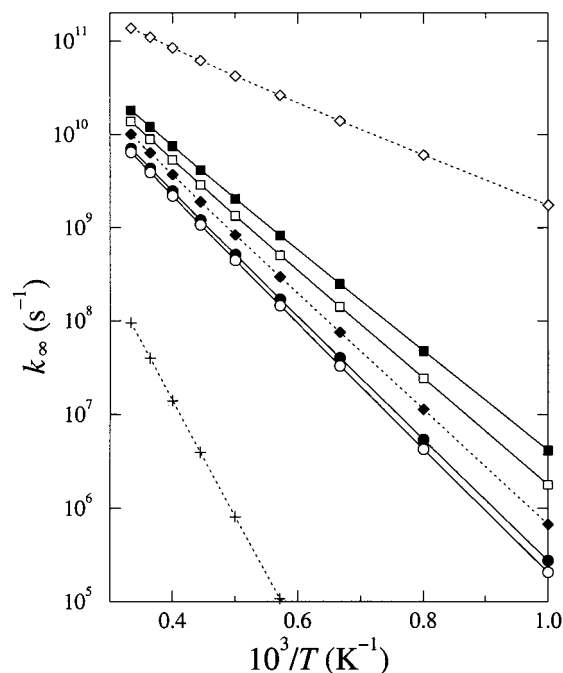


Figure 3. G2MP2 components' high-pressure-limit rate coefficients of the forward reaction 1, k_{∞} . The rate coefficients correspond to the Hartree–Fock {plus, dashed line}, PMP2(Full) {solid diamond, dashed line}, UMP2(Full) {open diamond, dashed line} procedural steps. Also included are the G2MP2 {solid circle, solid line}, G2PMP2 {open circle, solid line} (see text for explanation), G2MP2^{planar} {solid square, solid line}, and G2PMP2^{planar} {open square, solid line} results.

A comparison of the rate coefficients computed using the component methods of the G2MP2 method is shown in Figure 3. The HF value is very low, while the rate coefficient using the planar MP2(Full) calculation would give a very high reaction rate because of its erroneously low barrier. The spin projection has the opposite effect on the G2MP2 rate coefficients with the effect being limited to less than a factor of 2. This is due to a reversal of the relative barrier heights when comparing the restricted and unrestricted values. The planarity of the reactant changes the rate coefficients by an order of magnitude.

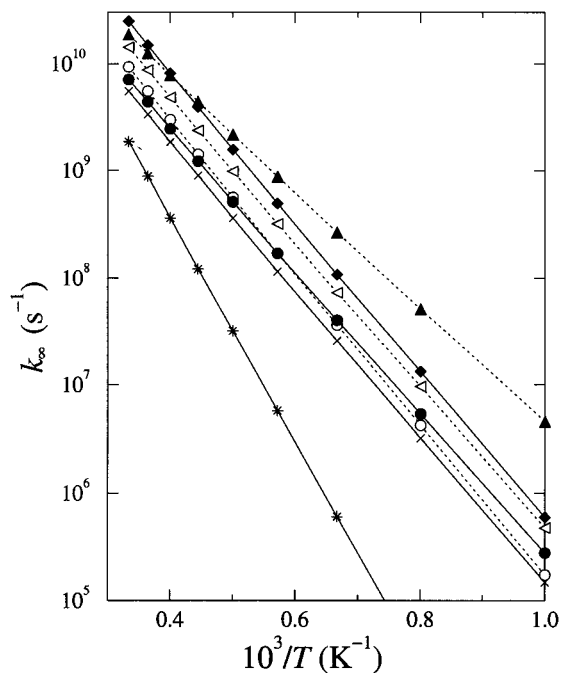


Figure 4. High-pressure-limit rate coefficients of the forward reaction 1, k_{∞} , for various methods and basis sets including PM3 {times, solid line}, MP2/6-31G(d) {open circle, dashed line}, B3-LYP/6-31G(d) {open left triangle, dashed line}, CBS-4 {solid up triangle, dashed line}, CASSCF(7,7)/6-31G(d) {star, solid line}, CASPT2/6-31G(d) {solid diamond, solid line}, and G2MP2 {solid circle, solid line}.

A plot of the high-pressure-limit rate coefficients computed with the data from the more reliable theoretical methods is given in Figure 4. The G2MP2 rate coefficients, with the additional attention to the MP2(Full) geometry optimization being a global minimum, are in the middle of the range. The CASSCF rate coefficients are very similar to the HF results, while the rate coefficient determined using the CASPT2 data is the largest depicted. Given that CASPT2 provides uniform treatment of both radicals and transition states, this rate coefficient can be considered reasonable. The CBS-4 rate coefficients are larger again because of the lower reaction barrier.

The effect of the frequency multiplier was found to have little influence on the final rate coefficients for any of the methods. The difference was determined to be less than 1.5% when raw frequencies are used compared to the scaled frequencies. As a sensitivity test, when the low frequencies were halved and doubled, the resulting change in the rate coefficients was less than 0.5%. The largest order-of-magnitude effect was due to the replacement of low vibrational modes with internal rotors.

5.3. Equilibrium Constants. We also investigated the equilibrium constant of reaction 1 with the same sample of quantum mechanical techniques as those used for rate coefficients. Figure 5 and Table 6 report the equilibrium constants, K_{eq} , for a number of theoretical methods. The sensitivity of the equilibrium constants to the quantum mechanical data is similar to the rate sensitivities. Most methods predict K_{eq} values less than unity, while the MP2/6-31G(d,p), CASSCF(7,7)/6-31G(d), and CASPT2/6-31G(d)/CASSCF(7,7)/6-31G(d) results yield values, in general, slightly greater than 1. Most disconcerting of all is the wide range of values and even the temperature dependence. The G2(P)MP2^{planar} results are in agreement with the MP2 and B3LYP values, but the nonplanar G2MP2 values are considerably smaller. The PM3 calculations produce an even smaller result.

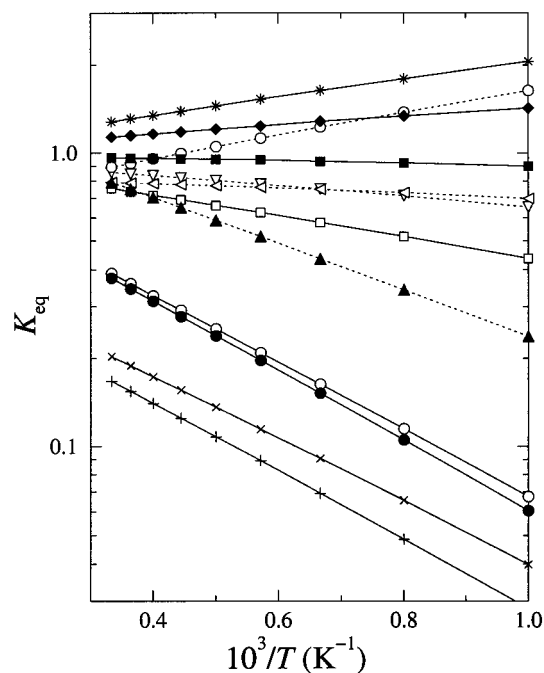


Figure 5. Equilibrium constants, K_{eq} , for reaction 1 obtained from calculations using various methods and basis sets. The semiempirical methods, AM1 {plus, solid line} and PM3 {times, solid line} are compared to ab initio methods, HF/6-31G(d) {open down triangle, dashed line}, MP2/6-31G(d,p) {open circle, dashed line}, B3-LYP/6-31G(d) {open left triangle, dashed line}, CBS-4 {solid up triangle, dashed line}, CASSCF/6-31G(d) {star, solid line}, and CASPT2/6-31G(d) {solid diamond, solid line}. Also included are the G2PMP2^{planar} {open square, solid line}, G2MP2 {open circle, solid line}, G2MP2^{planar} {solid square, solid line}, and G2MP2 {solid circle, solid line} method results.

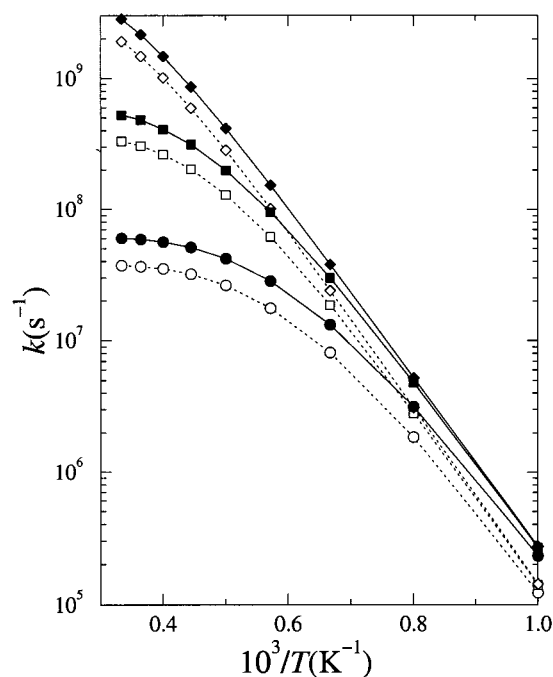


Figure 6. Forward rate coefficients of reaction 1 at three pressures using the PM3 {open symbols} and G2MP2 {solid symbols} data. The three pressures are 76 Torr {circles}, 760 Torr {squares}, and 7600 Torr {diamonds}.

5.4. Falloff. By use of the G2MP2 results with nonplanar geometry and semiempirical results for comparison, rate coefficients (Figure 6) for three pressures covering the range of

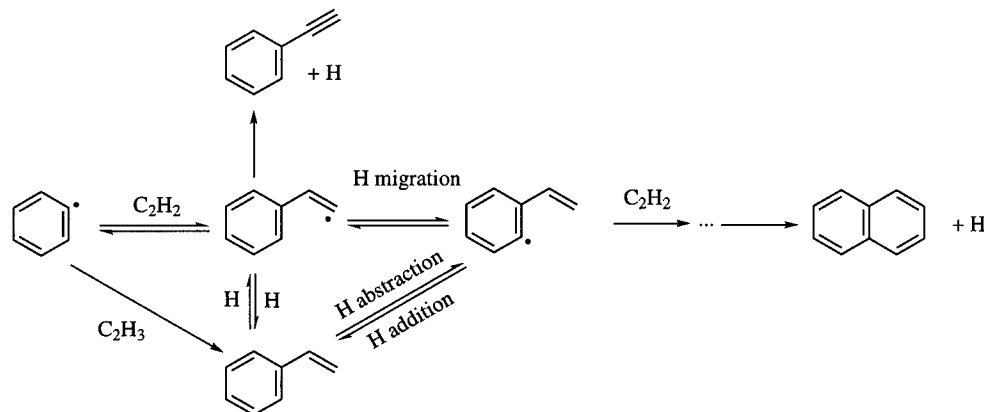


Figure 7. Reaction path diagram showing the role of the H migration of reaction 1 in the overall reaction path from phenyl to naphthalene.

TABLE 7: Coefficients of the Polynomial Fit, $a_0 + a_1T + a_2T^2 + a_3T^3 + a_4T^4 + a_5T^5$ Where T Is Temperature in K, of the Parameters in Eq 3 for Temperature and Pressures Ranges 500–2500 K and 10^{-5} – 10^3 atm, Respectively

| coefficients | parameters | | |
|--------------|--------------------------|--------------------------|--------------------------|
| | h | α | σ |
| a_0 | 1.458×10^{-01} | -5.829 | 7.693 |
| a_1 | 1.210×10^{-03} | 3.588×10^{-02} | -2.048×10^{-02} |
| a_2 | -7.159×10^{-07} | -7.209×10^{-05} | 5.155×10^{-05} |
| a_3 | -2.243×10^{-10} | 5.764×10^{-08} | -4.704×10^{-08} |
| a_4 | 2.362×10^{-13} | -2.017×10^{-11} | 1.772×10^{-11} |
| a_5 | -4.288×10^{-17} | 2.592×10^{-15} | -2.382×10^{-15} |

practical interest (in combustion) were determined using RRKM theory. The results based on the two quantum methods are very similar mostly because the high-pressure-limit rate coefficients are close. Both exhibit clear falloff behavior.

The falloff range of this reaction calculated by RRKM using the G2MP2 data was parametrized following Kazakov et al.⁴⁰ The unimolecular rate coefficient is approximated by interpolation between the low- and high-pressure limits, k_0 and k_∞ , as

$$k_{\text{falloff}} = \{(k_0[M])^a + k_\infty^a\}^{1/a} \quad (2)$$

where $[M]$ is the total gas density and a is a fitted function of temperature and pressure (or gas density),

$$a = h \exp\left(\left\{\log_{10} \frac{k_0[M]}{k_\infty} - \alpha\right\}/\sigma\right)^2 - 1 \quad (3)$$

The high- and low-pressure limits calculated with the G2MP2 data are, respectively, $k_\infty = (5.23 \times 10^9)T^{0.692} \exp(-14200/T) \text{ s}^{-1}$ (Table 6) and $k_0 = (3.32 \times 10^{15})T^{-0.242} \exp(-3480/T) \text{ cm}^3 \text{ mol}^{-1} \text{ s}^{-1}$. The “parameters” h , α , and σ of eq 3 were fitted with fifth-order polynomials in temperature (Table 7), matching the RRKM results computed using the G2MP2 information over the temperature and pressure ranges 500–2500 K and 10^{-5} and 10^3 atm, respectively. This representation was found to be largely within 1% error compared to the RRKM calculations, with a maximum deviation of 1.19%.

6. Mechanistic Implications

The rate coefficients computed here for reaction 1 at an ab initio level of quantum theory are comparable in value to the PM3 results. The latter was argued¹¹ to be sufficiently large for the H migration of the type portrayed by reaction 1 to compete with what presently is thought to be the primary reaction channels for aromatic growth.

For large aromatic structures, like condensed multi-ring soot precursors or those developed at the edges of soot particle surface, the H migration step opens an additional and somewhat faster reaction pathway, with an outcome of at least doubling the rate of cyclization.¹¹ The effect of an additional channel is rather straightforward because the cyclization reaction in this case takes place at the aromatic bay with a large decrease in the Gibbs free energy and hence is essentially *irreversible*.

For smaller aromatics, the cyclization process involves a sequence of tightly balanced reversible reaction steps,⁴ like those shown in Figure 7. The equilibrium constant of near-unity computed for reaction 1 further accentuates the key mechanistic feature governing the process, the coupling between a kinetic driving force and thermodynamic resistance to growth.^{4,41} In other words, the rapid hydrogen migration, reaction 1, reasserts the state of partial equilibrium among aromatic radical intermediates. As a result, reaction 1 not only accelerates the aromatic growth, via its forward direction, but also promotes fragmentation, through its reverse.

One possible outcome of the rapidly equilibrating reaction 1 is the following. Assuming that we start with phenyl and a large concentration of vinyl, their combination would form styrene, as shown in Figure 7. A hydrogen abstraction from the ring forms a 2-styrenyl radical, whose combination with acetylene (or vinyl in this case) may lead to the formation of the second aromatic ring. One would assume then that this direct formation of 2-styrenyl via styrene should dominate the acetylene addition pathway in a vinyl-rich environment. This is indeed what was obtained in early kinetic simulations.⁴² However, the vinyl-addition pathway was prominent only in the very initial phase of the reaction. With the buildup of acetylene concentration, the main growth was shown to switch to the acetylene-addition route. The present results indicate that the switch may occur even faster because of the decomposition of 2-styrenyl via the reverse direction of reaction 1.

7. Conclusions

Many levels of quantum theory and basis sets were tested on the hydrogen migration reaction in phenylethen-2-yl to give 2-styrene (reaction 1). Several criteria were used to determine the method of choice for predicting accurate kinetics information. The theoretical foundation, spin contamination, and previously determined agreement with experiment were taken into consideration.

On the basis of the low-spin contamination and agreement with other reliable methods, the chemically accurate G2MP2 method, which also has been tested for a large data set,²⁷ is our top choice. Among the other methods tested, the B3-LYP,

CASPT2//CASSCF, and MP2 methods using the 6-31G(d,p) basis set give results in agreement with the G2MP2 method and could be used to reduce computational expense. Note, however, that the MP2 method was the only calculation to produce nonplanar geometries for the reactant and product.

The calculation of reaction rate coefficients and equilibrium constants was most sensitive to the potential energy barriers predicted by different levels of theory and to the replacement of low-frequency vibrational modes by free internal rotors. The range is discomfortingly large in the predictions for the reaction coefficient, k , and in particular, the equilibrium constant, K_{eq} , even among the better methods tested in this study.

At the G2MP2 level of theory, our top choice, the results are $k_{\infty} = (5.23 \times 10^9)T^{0.692} \exp(-14200/T) \text{ s}^{-1}$ and $k_0 = (3.32 \times 10^{15})T^{-0.242} \exp(-3480/T) \text{ cm}^3 \text{ mol}^{-1} \text{ s}^{-1}$, while the falloff behavior is described by eq 3 and Table 7. These results are comparable in magnitude to the presently known rates of key aromatic-growth reactions. The hydrogen migration investigated here opens an additional channel to aromatic ring growth and ring fragmentation.¹¹ We thus conclude that the title reaction should play an important role in the chemistry of polycyclic aromatic ring growth and destruction.

Acknowledgment. The research was supported by the Director, Office of Science, Office of Basic Energy Sciences, Chemical Sciences Division of the U.S. Department of Energy, under Contract No. DE-AC03-76SF00098. Calculations were performed, in part, at the National Energy Research Scientific Computing (NERSC) Center.

References and Notes

- Haynes, B. S.; Wagner, H. G. *Prog. Energy Combust. Sci.* **1981**, *7*, 229.
- Bockhorn, H., Ed. *Soot Formation in Combustion: Mechanisms and Models*; Springer-Verlag: Berlin, 1994.
- Bittner, J. D.; Howard, J. B. *Symp. (Int.) Combust., [Proc.]*, **18th** **1981**, 1105.
- Frenklach, M.; Clary, D. W.; Gardiner, W. C., Jr.; Stein, S. E. *Symp. (Int.) Combust., [Proc.]*, **20th** **1985**, 887.
- Frenklach, M.; Wang, H. *Symp. (Int.) Combust., [Proc.]*, **23rd** **1991**, 1559.
- Colket, M. B.; Hall, R. J. In *Soot Formation in Combustion: Mechanisms and Models*; Bockhorn, H., Ed.; Springer-Verlag: Berlin, 1994; p 442.
- Colket, M. D.; Seery, D. J. *Symp. (Int.) Combust., [Proc.]*, **22nd** **1994**, 883.
- Melius, C. F.; Colvin, M. E.; Marinov, N. M.; Pitz, W. J.; Senkan, S. M. *Symp. (Int.) Combust., [Proc.]*, **26th** **1996**, 685.
- Wang, H.; Frenklach, M. *Combust. Flame* **1997**, *110*, 173.
- Marinov, N. M.; Pitz, W. J.; Westbrook, C. K.; Vincitore, A. M.; Castaldi, M. J.; Senkan, S. M.; Melius, C. F. *Combust. Flame* **1998**, *114*, 192.
- Frenklach, M.; Moriarty, N. W.; Brown, N. J. *Symp. (Int.) Combust., [Proc.]*, **27th** **1998**, 1655.
- Stewart, J. J. P. *J. Comput. Chem.* **1989**, *10*, 209.
- Stewart, J. J. P. *J. Comput. Chem.* **1989**, *10*, 221.
- Pople, J. A.; Nesbet, R. K. *J. Chem. Phys.* **1959**, *22*, 571.
- Möller, C.; Plesset, M. S. *Phys. Rev.* **1934**, *46*, 618.
- Becke, A. D. *J. Chem. Phys.* **1993**, *98*, 5648.
- Lee, C.; Yang, W.; Parr, R. G. *Phys. Rev. B* **1988**, *37*, 785.
- Mebel, A. M.; Morokuma, K.; Lin, M. C. *J. Chem. Phys.* **1995**, *103*, 7414.
- Mayer, P. M.; Parkinson, C. J.; Smith, D. M.; Radom, L. *J. Chem. Phys.* **1997**, *108*, 604.
- Wong, M. W.; Radom, L. *J. Phys. Chem. A* **1998**, *102*, 2237.
- Curtiss, L. A.; Raghavachari, K.; Pople, J. A. *J. Chem. Phys.* **1993**, *98*, 1293.
- Eade, R. H. E.; Robb, M. A. *Chem. Phys. Lett.* **1981**, *83*, 362.
- McDouall, J. J.; Peasley, K.; Robb, M. A. *Chem. Phys. Lett.* **1988**, *148*, 183.
- Andersson, K.; Roos, B. O.; Malmqvist, P.-Å.; Widmark, P.-O. *Chem. Phys. Lett.* **1994**, *230*, 391.
- Dewar, M. J. S.; Zebisch, E. G.; Healy, E. F. *J. Am. Chem. Soc.* **1985**, *106*, 3902.
- Ochterski, J. W.; Petersson, G. A.; Montgomery, J. A., Jr. *J. Chem. Phys.* **1996**, *104*, 2598.
- Curtiss, L. A.; Trucks, G. W.; Raghavachari, K.; Pople, J. A. *J. Chem. Phys.* **1991**, *94*, 7221.
- Pople, J. A.; Head-Gordon, M.; Raghavachari, K. *J. Chem. Phys.* **1987**, *87*, 7382.
- Frisch, M. J.; Trucks, G. W.; Schlegel, H. B.; Gill, P. M. W.; Johnson, B. G.; Robb, M. A.; Cheeseman, J. R.; Keith, T.; Petersson, G. A.; Montgomery, J. A.; Raghavachari, K.; Al-Laham, M. A.; Zakrzewski, V. G.; Ortiz, J. V.; Foresman, J. B.; Cioslowski, J.; Stefanov, B. B.; Nanayakkara, A.; Challacombe, M.; Peng, C. Y.; Ayala, P. Y.; Chen, W.; Wong, M. W.; Andres, J. L.; Replogle, E. S.; Gomperts, R.; Martin, R. L.; Fox, D. J.; Binkley, J. S.; Defrees, D. J.; Baker, J.; Stewart, J. P.; Head-Gordon, M.; Gonzalez, C.; Pople, J. A. *Gaussian 94*; Gaussian, Inc.: Pittsburgh, PA, 1995.
- Andersson, K.; Blomberg, M. R. A.; Fülscher, M. P.; Karlström, G.; Lindh, R.; Malmqvist, P.-Å.; Neogrády, P.; Olsen, J.; Roos, B. O.; Sadlej, A. J.; Schütz, M.; Seijo, L.; Serrano-Andrés, L.; Siegbahn, P. E. M.; Widmark, P.-O. *Molcas*, version 4; Theoretical Chemistry, Lund University: Lund, Sweden, 1997.
- Stewart, J. J. P. Quantum Chemistry Exchange Program No. 455, Indiana University, Bloomington, IN, 1983. Stewart, J. J. P. *CS Chem3D Pro 3.5*; CambridgeSoft: Cambridge, MA, 1996.
- Tsuzuki, S.; Tanabe, K.; Osawa, E. *J. Phys. Chem.* **1990**, *94*, 6175.
- Head-Gordon, M.; Pople, J. A. *J. Phys. Chem.* **1993**, *97*, 1147.
- Hargiti, R.; Szalay, P. G.; Pnogor, G.; Foragasi, G. *J. Mol. Struct.: THEOCHEM* **1994**, *306*, 293.
- Zilberg, S.; Haas, Y. *J. Chem. Phys.* **1995**, *103*, 20.
- Scott, A. P.; Radom, L. *J. Phys. Chem.* **1996**, *100*, 16502.
- Holbrook, K. A.; Pilling, M. J.; Robinson, P. J. *Unimolecular Reactions*; Wiley: New York, 1996.
- Gilbert, R. G.; Smith, S. C. *Theory of Unimolecular and Recombination Reactions*; Blackwell-Scientific: Oxford, 1990.
- Wang, H.; Frenklach, M. *Combust. Flame* **1994**, *96*, 163.
- Kazakov, A.; Wang, H.; Frenklach, M. *J. Phys. Chem.* **1994**, *98*, 10598.
- Frenklach, M. *Symp. (Int.) Combust., [Proc.]*, **22nd** **1989**, 1075.
- Frenklach, M.; Clary, D. W.; Gardiner, W. C., Jr.; Stein, S. E. *Symp. (Int.) Combust., [Proc.]*, **21st** **1988**, 1067.